Polarization-dependent nonlinear refraction and two-photon absorption in GaAs/AlAs superlattice waveguides below the half-bandgap

Sean J. Wagner,[1,*] Joachim Meier,[1] A. S. Helmy,[1] J. Stewart Aitchison,[1] Marc Sorel,[2] and David C. Hutchings[2]

[1]*Edward S. Rogers Sr. Department of Electrical and Computer Engineering, University of Toronto, Toronto, Ontario M5S 3G4, Canada*

[2]*Department of Electronics & Electrical Engineering, University of Glasgow, Glasgow G12 8QQ, Scotland, UK*

[*]*Corresponding author: sean.wagner@utoronto.ca*

Received September 29, 2006; accepted January 8, 2007;
posted March 23, 2007 (Doc. ID 75599); published June 15, 2007

Values for the two-photon absorption coefficient, α_2, and nonlinear refractive index coefficients, n_2, are measured for a waveguide core made of 14:14 monolayer GaAs/AlAs superlattice at photon energies below the half-bandgap. Two-photon absorption coefficients show significant anisotropy with the TE mode having α_2 values up to four times greater than the TM mode. For nonlinear refraction, we determined values of the nonlinear index for the TE mode that are as much as two times larger than the TM mode. Measurements of cross-phase modulation between the TE and TM modes gave ratios of cross-phase modulation to self-phase modulation that were highly anisotropic. © 2007 Optical Society of America

OCIS codes: 190.5970, 160.4330.

1. INTRODUCTION

Compound semiconductors and AlGaAs, in particular, have opened many possibilities for all-optical signal processing by nonlinear optical phenomena. They have mature fabrication technologies, and the magnitude of the Kerr effect in AlGaAs is ~500 times stronger than in silica fibers [1]. This allows devices such as ultrafast nonlinear directional couplers [2,3] to be scaled into compact forms for integration with other components on the same chip. Multiple quantum well (MQW) and superlattices in the GaAs/AlGaAs material system have drawn interest as nonlinear materials because of the ability to selectively tune the bandgap and nonlinear properties using post-growth techniques such as quantum-well intermixing (QWI) [4]. Short-period superlattices have the advantage that complete intermixing yields the largest possible modification in the bandgap and nonlinear properties [5]. Changes may be large enough that the nonlinearity can be reduced to the point where the material becomes relatively linear. Thus, intermixing can be used to pattern areas on a semiconductor chip that are optically linear or nonlinear. GaAs/AlAs superlattices and QWI have already been used to fabricate quasi-phase-matching structures for controlling second-order nonlinear processes [6,7]. The third-order nonlinear properties of the GaAs/AlAs superlattice are of great interest since nonlinear refraction in GaAs/AlGaAs MQWs has shown enhancement of the polarization dependence over bulk AlGaAs [8]. However, detrimental nonlinear absorption processes such as two-photon absorption (TPA) are strengthened in quantum-well structures. Optimal devices should be operated below but near the half-bandgap to take advantage of large nonlinear refraction while limiting TPA.

The physical asymmetry in a multilayer heterostructure such as a superlattice has the immediate consequence of introducing anisotropy in the optical properties of the structure. Translational symmetry is broken along the [001] growth direction, thus making the optical properties of the material dependent on the crystallographic direction. Breaking symmetry leads to new, nonzero elements in the electric susceptibility tensors. In the third-order susceptibility tensor for the single wavelength case, the three independent nonzero components of bulk zinc-blende semiconductors break into eight elements. For light propagating in the [110] direction (the usual waveguide orientation), four of these elements are involved in self-phase modulation (SPM): $\chi^{(3)}_{xxxx}$, $\chi^{(3)}_{xyxy}$, and $\chi^{(3)}_{xxyy}$ for the TE polarization, and $\chi^{(3)}_{zzzz}$ for the TM polarization. Two elements are involved in cross-phase modulation (XPM) between both polarizations: $\chi^{(3)}_{xzxz}$ for TE and $\chi^{(3)}_{zxzx}$ for TM. Predicted values of the tensor components vary in magnitude and lead to a highly polarization-dependent nonlinear index of refraction [9]. Significant birefringence in the linear index of refraction has already been experimentally verified for a superlattice [10]. Furthermore, the degeneracy between the light- and heavy-hole valence bands is lifted in quantum heterostructures, and therefore the bandgaps involving the heavy- and light-hole bands differ in energy. Since linear transitions from the heavy-hole band are forbidden for the linear polarization along the [001] direction but allowed for the [110] direction, the linear absorption peaks for TE- and TM-polarized light will be found at different wavelengths. Thus, the location of

the half-bandgap and behavior of the associated nonlinear properties, such as TPA and nonlinear refractive index, will be different for each polarization.

In this paper, we experimentally determine the third-order nonlinear optical properties of a waveguide core made of a nonintermixed 14:14 monolayer GaAs/AlAs superlattice at wavelengths below its half-bandgap. The linear properties are examined to estimate their impact on the nonlinear behavior of these waveguides. Measurements of TPA are carried out by using the inverse transmission method [1]. Nonlinear refraction is examined for the case of SPM involving one linear polarization, and XPM involving the interaction between both polarizations. Coefficients for SPM and XPM are obtained from observations of SPM- and XPM-induced spectral broadening and comprehensive modeling of nonlinear pulse propagation. In the case of XPM, we account for the group velocity mismatch between the TE and TM modes that causes the spectrum to broaden asymmetrically about the center wavelength. For both TPA and nonlinear refraction, we also isolate the nonlinear behavior of the superlattice layer from the waveguide structure by accounting for the nonlinear behavior of the cladding layers.

2. STRUCTURE AND LINEAR PROPERTIES OF SUPERLATTICE WAVEGUIDES

To evaluate the nonlinear properties of the superlattice, it was necessary to measure several of the linear properties of the waveguides. This included the room-temperature photoluminescence to verify the bandgap energy, the transverse profiles of the guided modes, and the linear loss. The wafer structure shown in Fig. 1 was devised to optimize second-harmonic generation from a 1550 nm fundamental [5] and was characterized previously [10]. It consisted of a 0.6 μm thick GaAs/AlAs superlattice core layer with 75 periods of 14:14 monolayers each. Buffer layers of 0.3 μm thick $Al_{0.56}Ga_{0.44}As$ were placed on either side of the superlattice to increase the mode size and hence the coupling efficiency from objective lenses. Upper and lower cladding layers were $Al_{0.60}Ga_{0.40}As$ with thicknesses of 0.8 and 4.0 μm, respectively. All layers were grown nominally undoped by molecular beam epitaxy on a semi-insulating GaAs substrate. Strip-loaded waveguides, each 3 μm wide and etched to a depth of 0.8 μm, were fabricated using reactive-ion etching.

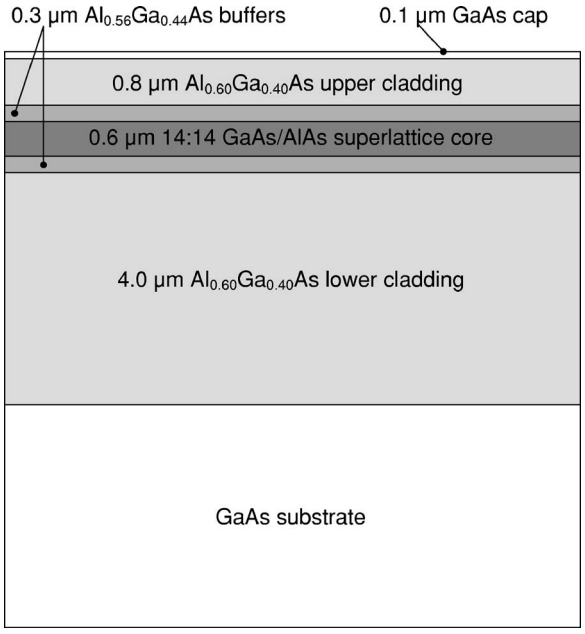

Fig. 1. Layer structure of the superlattice-core waveguide wafer.

The room-temperature photoluminescence peaks of the superlattice layer were measured for each polarization. Light from a frequency-doubled Nd:YAG laser emitting at 532 nm was scanned along the cross section of the wafer. Re-emitted light from the wafer was passed through polarization filters before detection. For TE-polarized light, the photoluminescence peak of the superlattice layer was located at 753 nm (~1.65 eV), and for TM-polarized light, it was found at 730 nm (~1.70 eV), confirming the lifted degeneracy of the light- and heavy-hole valence bands. For both polarizations, the half-bandgap is close to 1500 nm, making this material suitable for devices operating at optical communications wavelengths with an expected minimal loss contribution from TPA.

A commercial mode solver from Lumerical Solutions, Inc. was used to find the mode profiles of the waveguides for the TE and TM polarizations. The linear refractive indices of the $Al_{0.56}Ga_{0.44}As$ and $Al_{0.60}Ga_{0.40}As$ layers were obtained from the empirical model of Gehrsitz *et al.* [11]. Values for the linear index of refraction for the superlattice were derived from effective index values of this layer structure reported by Kleckner *et al.* [10]. Analysis of the TE mode profiles showed that ~50% of the power is confined to the superlattice layer, and 30% of the power is found in the buffer layers. The TM mode confines only 38% of the power to the superlattice layer, which results from the lower index contrast between the cladding and the superlattice for TM-polarized light. Increased confinement of the TE mode brings higher optical intensities and thus stronger nonlinear effects compared with the TM mode for the same optical power.

Linear losses for these waveguides were experimentally determined using the Fabry–Perot method for wavelengths between 1505 and 1640 nm. The loss coefficients for the TE mode were measured as 0.25 cm^{-1} while the TM mode had a larger loss coefficient of 0.7 cm^{-1}. We attribute this increased loss in the TM modes to increased scattering and leakage losses incurred by reduced confinement of this mode to the waveguide core.

3. NONLINEAR OPTICAL MEASUREMENTS

In the waveguide structure studied here, the guided modes were not completely confined to the superlattice layer. The buffer and cladding layers contributed to the nonlinear behavior of the waveguide as a whole. To isolate the nonlinear behavior of the superlattice itself, it was necessary to account for the contributions from the bulk AlGaAs layers in the measured data. Using the formalism of Grant [12], the total effective change in the index of refraction due to third-order nonlinear refraction is

$$\Delta n_{eff} = \frac{n_{2,(1)} \int\int_{(1)} I^2(x,y)\mathrm{d}x\mathrm{d}y + n_{2,(2)} \int\int_{(2)} I^2(x,y)\mathrm{d}x\mathrm{d}y + \cdots}{\int_{-\infty}^{\infty}\int_{-\infty}^{\infty} I(x,y)\mathrm{d}x\mathrm{d}y}, \tag{1}$$

where $I(x,y)$ is the transverse profile of the irradiance, and $n_{2,(i)}$ is the nonlinear refraction coefficient for material i of the waveguide structure. Equation (1) can be rewritten as

$$\Delta n_{eff} = n_{2,(1)} \frac{P}{A^{(3)}_{eff,(1)}} + n_{2,(2)} \frac{P}{A^{(3)}_{eff,(2)}} + \cdots, \tag{2}$$

where P is the optical power, and

$$A^{(3)}_{eff,(i)} = \frac{\left[\int_{-\infty}^{\infty}\int_{-\infty}^{\infty} I(x,y)\mathrm{d}x\mathrm{d}y\right]^2}{\int\int_{(i)} I^2(x,y)\mathrm{d}x\mathrm{d}y} \tag{3}$$

is the third-order effective area for material layer i. Given a particular structure, all the $A^{(3)}_{eff,(i)}$ values can be determined from a mode solver and hence the n_2 of any one material can be found given known n_2 values for the other materials. Similar equations for TPA can be derived by replacing n with α in Eqs. (1) and (2).

Nonlinear coefficients for nonlinear refraction in the bulk AlGaAs layer were calculated from known values n_2 for $Al_{0.18}Ga_{0.82}As$ [1] by using the direct bandgap energies from the model of Adachi [13] and the scaling laws for direct III–V semiconductors [14]. The resulting coefficients for $Al_{0.56}Ga_{0.44}As$ and $Al_{0.60}Ga_{0.40}As$ were calculated to be between 18% and 25% that of $Al_{0.18}Ga_{0.82}As$. While these compositions of AlGaAs have indirect bandgaps, calculations using the model of Dinu [15] showed that the contributions of the indirect transition to nonlinear refraction are negligible. In the case of TPA, the wavelengths used were at photon energies well below the half-bandgap of $Al_{0.56}Ga_{0.44}As$ and $Al_{0.60}Ga_{0.40}As$ where TPA is effectively zero. Thus, the contribution of these layers to nonlinear absorption was ignored.

The effective mode areas were calculated by using the solved mode profiles. For the superlattice core layer, $A^{(3)}_{eff,\mathrm{core}}$ was calculated to be between 9.7 and 11.2 μm^2 in the TE mode and between 16 and 24 μm^2 in the TM mode for wavelengths between 1500 and 1600 nm. As with the confinement factor, the difference in the mode areas is the result of the birefringence in the superlattice layer.

Characterization of the nonlinear properties was carried out using a singly resonant KTP optical parametric oscillator (OPO) synchronously pumped by a mode-locked Ti:sapphire laser. Output pulses had full width at half maximum (FWHM) lengths of 1.5 to 2.5 ps with a 75.6 MHz repetition rate and a maximum average power of 150 mW. Infrared light between 1505 and 1625 nm was end-fire coupled into a 1.2 cm long sample with an antireflection-coated 40× objective lens. The output of the waveguides was focused onto a power meter to measure the amount of transmission through the samples and onto an optical spectrum analyzer to track changes in the output spectrum.

A. Two-Photon Absorption

Two-photon absorption coefficients were determined for TE and TM polarizations with photon energies below the half-bandgap. While two-photon transitions should not occur below the half-bandgap, band tail states can lead to significant nonlinear absorption. To measure TPA, the transmission through the waveguides was recorded as a function of the input power at several wavelengths. The TPA coefficient, α_2, is related to the inverse of the transmission T by

$$\frac{1}{T} = \frac{1}{T_0} + \alpha_2 \frac{[1-\exp(-\alpha_1 L)]}{\alpha_1 (1-R)\exp(-\alpha_1 L)} I^{(3)}_{eff}, \tag{4}$$

where T_0 is the intercept with the $1/T$ axis, α_1 is the linear loss coefficient, R is the reflectivity of the facets, and $I^{(3)}_{eff} = P/A^{(3)}_{eff}$ is the effective intensity. By measuring the slope of the inverse transmission plot, the value of the TPA coefficient was calculated by Eq. (4). Since only the superlattice layer should contribute to TPA, $I^{(3)}_{eff}$ was calculated by using the superlattice core effective mode area.

Figure 2 shows the value of α_2 for the superlattice layer at several wavelengths. At 1545 nm, α_2 is 1.94 cm/GW for the TE mode and 0.94 cm/GW for the TM mode. In both polarizations, TPA is enhanced over bulk $Al_{0.18}Ga_{0.82}As$ [1] by up to four times. In the TE mode, α_2 increases rapidly as the half-bandgap of ~1500 nm is approached. The value of α_2 does not increase as rapidly for the TM mode since its half-bandgap is located at ~1460 nm. This difference in the bandgap leads to a large polarization dependence with the TE mode exhibiting TPA coefficients approximately six to nine times higher than that for the TM mode across the studied spectrum. Error in the values was the result of uncertainty in the calculated $A^{(3)}_{eff}$ values and measured pulse length.

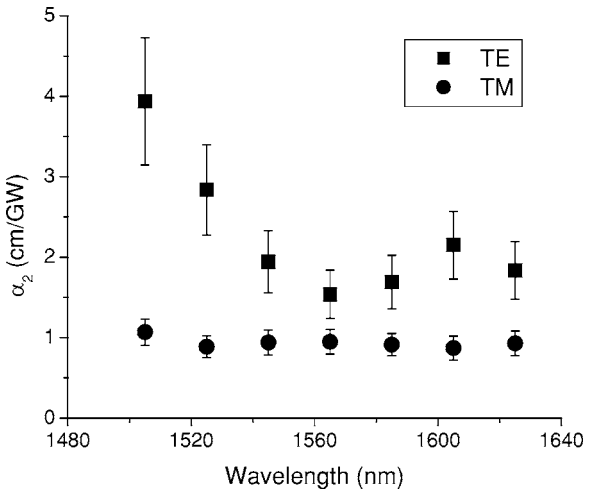

Fig. 2. Measured values of the two-photon absorption coefficient, α_2, for the TE and TM modes.

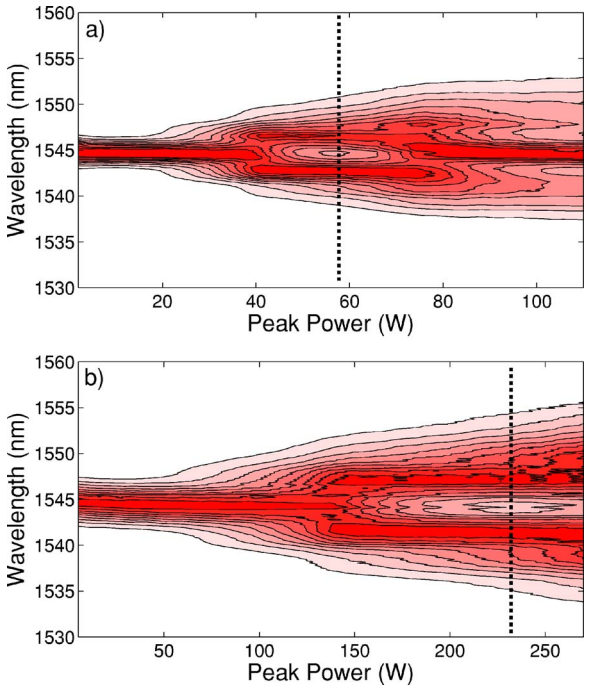

Fig. 3. (Color online) Measured SPM-induced spectral broadening at 1545 nm for the (a) TE mode and (b) TM mode. The dashed line indicates the input peak power at which the spectral broadening pattern corresponds to a 1.5π nonlinear phase shift.

B. Self-Phase Modulation

The nonlinear index of refraction was characterized by observing the spectral broadening induced by SPM. Figure 3 depicts the evolution of the measured output spectrum with increasing input peak power for TE and TM modes at a wavelength of 1545 nm. Pulse lengths of 2.5 ps were used for the TE mode while pulse lengths of 1.5 ps were used for the TM mode. While this widens the spectral width of the pulses for the TM mode experiments, this difference does not affect the shape of the spectral evolution in this pulse length regime. Thus, it is possible to make direct quantitative comparisons between the two polarizations. As the figures show, the spectrum splits apart into two peaks with a maximum dip in the middle. At this point, the phase shift is $\sim 1.5\pi$ [16]. The dotted lines show the position of this point, which occurs at ~ 58 W for the TE mode. The amount of power required to reach this same point in the TM mode is approximately four times larger. This difference is the result of reduced confinement and nonlinear strength in the TM mode.

To accurately determine the value of n_2 from the spectral measurements, it is necessary to account for dispersion, linear loss, and TPA. Propagation of an optical pulse through a nonlinear material is described by the nonlinear Schrödinger equation (NLSE) [17]:

$$j\frac{\partial A}{\partial z} + j\frac{\alpha_1}{2}A + j\frac{\alpha_2}{2}\frac{|A|^2}{A_{eff}^{(3)}}A - \frac{\beta_2}{2}\frac{\partial^2 A}{\partial t^2} + \frac{2\pi n_2}{\lambda A_{eff}^{(3)}}|A|^2 A = 0, \quad (5)$$

where $A(t,z)$ is the pulse envelope, z is the propagation distance, t is the retarded time, and β_2 is the group-velocity dispersion coefficient. The NLSE was solved numerically by using the split-step Fourier method [16]. Group-velocity dispersion coefficients calculated from the dispersion of the effective refractive index for the waveguides were of the order of $10^{-24}\,\mathrm{s}^2/\mathrm{m}$. The input pulses were modeled as chirped super-Gaussian of the form [16]:

$$A(t,0) = A_0 \exp\left[-\frac{1+iC}{2}\left(\frac{t}{t_0}\right)^{2m}\right], \quad (6)$$

where C is the chirp parameter, t_0 is the initial pulse width, and m is the super-Gaussian parameter. The values of C and m were set such that the simulations produced similar spectral evolution shapes as observed in experiments. Values of n_2 were determined by matching the power level at which the 1.5π phase-shift point occurs. An example of a simulation result matching the TE result of Fig. 3(a) is shown in Fig. 4 for the TE mode at 1545 nm. At 1545 nm, n_2 was determined to be $\sim 3.2 \times 10^{-13}\,\mathrm{cm}^2/\mathrm{W}$ for TE and $\sim 1.7 \times 10^{-13}\,\mathrm{cm}^2/\mathrm{W}$ for TM. Measured values of n_2 at other wavelengths are shown in Fig. 5 for both polarizations. As with α_2, nonlinear refraction is enhanced with coefficient values that are up to

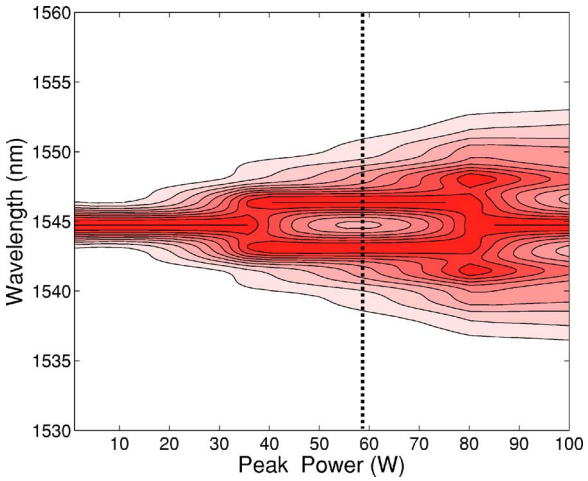

Fig. 4. (Color online) Simulated SPM-induced spectral broadening at 1545 nm for the TE mode produced by the split-step Fourier method. The evolution of the spectrum with input power and the location of the $3\pi/2$ nonlinear phase shift fits well with the measured spectral broadening of Fig. 3(a).

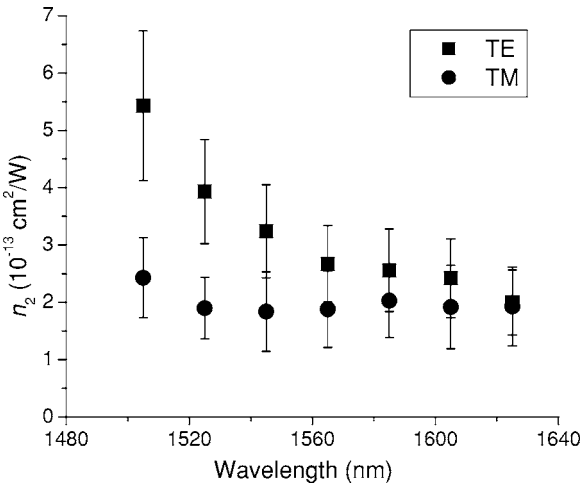

Fig. 5. Measured values of the nonlinear refractive index coefficient, n_2, for the TE and TM modes.

twice as large in bulk AlGaAs. The experimental values are larger than those predicted from models of the superlattice band structure [9]. The Kerr effect is highly anisotropic with the TE mode having an n_2 up to twice as large as the TM mode. In bulk AlGaAs waveguides, the difference between the polarizations is 27% at most [18]. The effect of the difference in the position of the electronic bandgap for the TE and TM polarizations is evident with the value of n_2 rapidly increasing as the TE half-bandgap is approached. At shorter wavelengths, the anisotropy agrees with the theoretical predictions of a three-times-enhanced nonlinearity for the TE polarization [9].

C. Cross-Phase Modulation

Measuring the coefficients related to XPM between the TE and TM polarizations is complicated by the large birefringence, which leads to a group-velocity mismatch between the polarizations. Furthermore, pulse shape and chirp can significantly affect XPM-induced spectral broadening and has not been taken into account previously when measuring similar bulk structures. In our simulations of copropagating orthogonally polarized pulses, we accounted for the temporal walk-off, pulse shape, and chirp.

For a sufficiently weak probe polarization, the propagation of two orthogonally polarized optical pulses through a nonlinear material is described by the coupled NLSEs [16]:

$$j\frac{\partial A_{pm}}{\partial z}+j\frac{\alpha_{pm}}{2}A_{pm}+j\frac{\alpha_{2,pm}}{2}\frac{|A_{pm}|^2}{A_{eff,pm}^{(3)}}A_{pm}-\frac{1}{v_{g,pm}}\frac{\partial A_{pm}}{\partial t}-\frac{\beta_{2,pm}}{2}\frac{\partial^2 A_{pm}}{\partial t^2}+\frac{2\pi}{\lambda}\frac{n_2}{A_{eff,pm}^{(3)}}|A_{pm}|^2A_{pm}=0, \tag{7}$$

$$j\frac{\partial A_{pb}}{\partial z}+j\frac{\alpha_{pb}}{2}A_{pb}-\frac{1}{v_{g,pb}}\frac{\partial A_{pb}}{\partial t}-\frac{\beta_{2,pb}}{2}\frac{\partial^2 A_{pb}}{\partial t^2}+\frac{2\pi}{\lambda}\frac{n_{X2}}{A_{eff,pm}^{(3)}}|A_{pm}|^2A_{pb}=0, \tag{8}$$

where the subscripts pm and pb denote the pump and probe, respectively. Four-wave mixing was ignored due to the large birefringence in the superlattice. The group-velocity terms containing $v_{g,pm}$ and $v_{g,pb}$ cause the pump and probe to walk off from each other in the time domain. Cross-phase modulation is accounted for with the term in Eq. (8) containing n_{X2}, the XPM nonlinear refraction coefficient. As with SPM, these equations were solved numerically by using the split-step Fourier method.

Cross-phase modulation was measured with a weak probe on one polarization and a strong pump on the other that were launched simultaneously into the superlattice waveguide. The probe was kept to no more than 7% of the power in the pump to limit SPM in the probe. The measured spectral broadening of the probe pulse is shown in Fig. 6 for the TM pump → TE probe configuration at 1545 nm. In this case, the TE probe had a lower group velocity and progressively lagged the TM pump over propagation through the waveguide. Due to the walk-off, the falling edge of the pump pulse acted on the probe pulse.

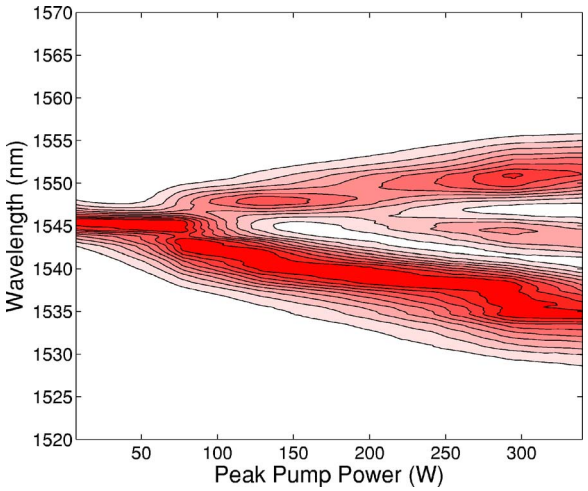

Fig. 6. (Color online) Measured XPM-induced spectral broadening of a 1545 nm TE mode probe acted on by a TM mode pump. Asymmetric broadening results from the group velocity mismatch between probe and pump.

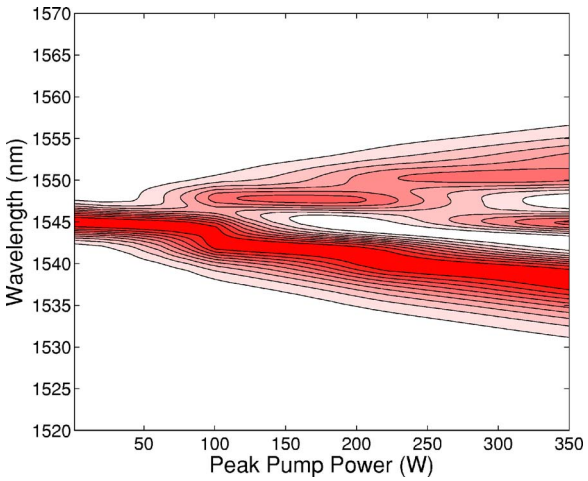

Fig. 7. (Color online) Simulated XPM-induced spectral broadening of a TE probe acted on by TM pump at 1545 nm. The broadening pattern matches well with the measured pattern in Fig. 7.

Since the change in the instantaneous optical frequency is related to the pulse envelope as [16]

$$\delta\omega \propto -\frac{\partial}{\partial t}|A(z,t)|^2, \tag{9}$$

the spectral components of the probe tend to shift toward higher frequencies. As a result, the spectral evolves asymmetrically with more of the probe power shifting toward blue as the pump power is increased. In the TE pump → TM probe case, the pump lagged the probe, and the probe spectrum broadened asymmetrically toward longer wavelengths.

Nonlinear refraction coefficients for XPM were obtained by matching measured spectrum changes with computer simulations of chirped super-Gaussian pulses propagated through a nonlinear medium. Group-velocity coefficients for these simulations were obtained from the measured dispersion of the refractive index for the superlattice [10]. Figure 7 shows a well-matched spectral

broadening pattern from the simulator for the TM pump → TE probe case at 1545 nm. The measured values of n_{X2} obtained by this method are shown in Fig. 8. The coefficients are of the same order of magnitude as values of n_2 for SPM. As with the SPM values, the experimental values are larger than those predicted [9]. The polarization dependence is apparent in the ratio of XPM to SPM, n_{X2}/n_2, which is shown in Fig. 9. The ratio is 0.75 ± 0.1 for TM pumps on TE probes and 0.43 ± 0.07 for TE pumps on TM probes. This agrees well with previous measurements of XPM in AlGaAs/GaAs MQW waveguides [19].

D. Device Implications

To evaluate the potential of the superlattice as a nonlinear material for all-optical switching devices, the strength of nonlinear refraction must be weighted with the detrimental effects of TPA. Here, the figure of merit used is defined as [20]

$$\mathrm{FOM} = \frac{2\alpha_2\lambda}{n_2}. \tag{10}$$

Figure 10 shows the value of the figure of merit for the wavelengths studied. The TM mode gives a better figure of merit with values that are closer to the desired value of 1. While the figure of merit is not as low as in bulk AlGaAs [1], this does not rule out the usefulness of the superlattice. Compared with the figure of merit for other semiconductors such as silicon [21] and AlGaAs/GaAs MQWs [8], the figure of merit for the investigated superlattice is better at wavelengths near 1550 nm by at least a factor of 2. Additionally, the high anisotropy in the Kerr coefficient is desirable for several types of polarization-dependent devices such as nonlinear Mach–Zehnder interferometers [22].

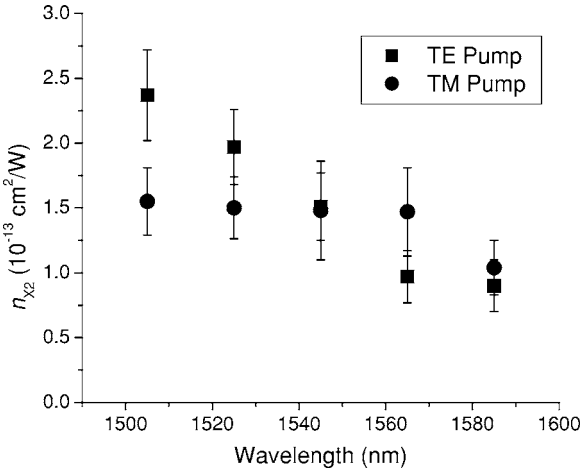

Fig. 8. Measured nonlinear refraction coefficients for XPM, n_{X2}, in the superlattice.

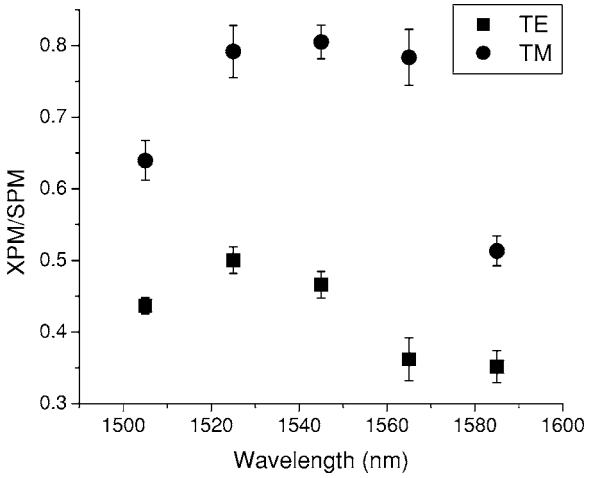

Fig. 9. Measured XPM–SPM ratios for the superlattice.

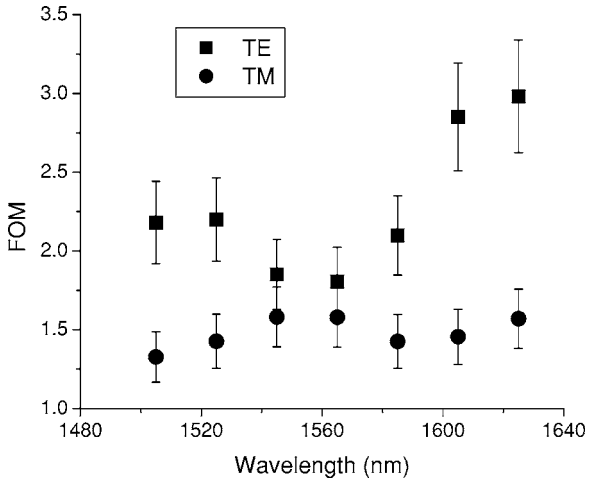

Fig. 10. Figure of merit for TE and TM modes.

The ability to intermix the superlattice as a technique for monolithic integration makes up for the reduced nonlinear performance. Selective control of the nonlinearity monolithically using QWI enables the integration of linear and nonlinear sections on the same chip and/or device. Applications include maximizing switching efficiency in nonlinear directional couplers and Mach–Zehnder interferometers, for example. Using the same technology to integrate active and passive devices may open a route for the integration of active and passive nonlinear elements.

Changes to the superlattice structure can be made to improve the figure of merit. The core layers adjacent to the buffer layers are GaAs quantum wells, and hence, this pair of asymmetric quantum wells with an energy separation between the lowest conduction state and highest valence state is smaller than the rest of the superlattice. Hence there will be a degree of parasitic TPA from these layers in the spectral region studied. A redesigned wafer with AlAs barrier layers adjacent to the buffer layers will eliminate this parasitic nonlinear loss.

4. CONCLUSIONS

In conclusion, we determined experimentally the third-order nonlinear optical properties of a GaAs/AlAs superlattice for wavelengths below the half-bandgap. The structure of the superlattice breaks symmetry, which brings new nonzero components in the third-order nonlinear electric susceptibility tensor. The difference in the absorption peaks for the TE and TM polarizations leads to further anisotropy in the optical properties. Two-photon absorption and the nonlinear index of refraction of the su-

perlattice were found to be enhanced over bulk AlGaAs. Both phenomena are highly anisotropic with the TE mode exhibiting stronger nonlinear effects due to closer proximity to the half-bandgap resonance. At appropriate optical power levels, the superlattice investigated can be considered a nonlinear medium in the TE polarization and a linear medium in the TM polarization. Cross-phase modulation showed similar polarization dependencies. While the figure of merit has a value that is larger than desired, the polarization dependence and the ability to modify the superlattice with QWI make the superlattice useful for nonlinear optics and photonic-integrated circuits.

ACKNOWLEDGMENTS

The authors thank D. Modotto for providing the split-step Fourier method software code used in this study. We also acknowledge the efforts of Philip Scrutton in providing the photoluminescence data.

REFERENCES

1. J. S. Aitchison, D. C. Hutchings, J. U. Kang, G. I. Stegeman, and A. Villeneuve, "The nonlinear optical properties of AlGaAs at the half band gap," IEEE J. Quantum Electron. **33**, 341–348 (1997).
2. J. S. Aitchison, A. H. Kean, C. N. Ironside, A. Villeneuve, and G. I. Stegeman, "Ultrafast all-optical switching in $Al_{0.18}Ga_{0.82}As$ directional coupler in 1.55 μm spectral region," Electron. Lett. **27**, 1709–1710 (1991).
3. A. Villeneuve, C. C. Yang, P. G. J. Wigley, G. I. Stegeman, J. S. Aitchison, and C. N. Ironside, "Ultrafast all-optical switching in semiconductor nonlinear directional couplers at half the band gap," Appl. Phys. Lett. **61**, 147–149 (1992).
4. J. H. Marsh, "Quantum well intermixing," Semicond. Sci. Technol. **6**, 1136–1155 (1993).
5. D. C. Hutchings and T. C. Kleckner, "Quasi phase matching in semiconductor waveguides by intermixing: optimization considerations," J. Opt. Soc. Am. B **19**, 890–894 (2002).
6. A. S. Helmy, D. C. Hutchings, T. C. Kleckner, J. H. Marsh, A. C. Bryce, J. M. Arnold, C. R. Stanley, J. S. Aitchison, C. T. A. Brown, K. Moutzouris, and M. Ebrahimzadeh, "Quasi phase matching in GaAs-AlAs superlattice waveguides through bandgap tuning by use of quantum-well intermixing," Opt. Lett. **25**, 1370–1372 (2000).
7. K. Zeaiter, D. C. Hutchings, R. M. Gwilliam, K. Moutzouris, S. V. Rao, and M. Ebrahimzadeh, "Quasi-phase-matched second-harmonic generation in a GaAs/AlAs superlattice waveguide by ion-implantation-induced intermixing," Opt. Lett. **28**, 911–913 (2003).
8. C. C. Yang, A. Villeneuve, G. I. Stegeman, C. H. Lin, and H. H. Lin, "Measurements of two-photon absorption coefficient and induced nonlinear refractive index in GaAs/AlGaAs multiquantum well waveguides," Electron. Lett. **29**, 37–38 (1993).
9. D. C. Hutchings, "Theory of ultrafast nonlinear refraction in semiconductor superlattices," IEEE J. Sel. Top. Quantum Electron. **10**, 1124–1132 (2004).
10. T. C. Kleckner, A. S. Helmy, K. Zeaiter, D. C. Hutchings, and J. S. Aitchison, "Dispersion and modulation of the linear optical properties of GaAs-AlAs superlattice waveguides using quantum-well intermixing," IEEE J. Quantum Electron. **42**, 280–286 (2006).
11. S. Gehrsitz, F. K. Reinhart, C. Gourgon, N. Herres, A. Vonlanthen, and H. Sigg, "The refractive index of $Al_xGa_{1-x}As$ below the band gap: accurate determination and empirical modeling," J. Appl. Phys. **87**, 7825–7837 (2000).
12. R. S. Grant, "Effective non-linear coefficients of optical waveguides," Opt. Quantum Electron. **28**, 1161–1173 (1996).
13. S. Adachi, "GaAs, AlAs, and $Al_xGa_{1-x}As$: material parameters for use in research and device applications," J. Appl. Phys. **58**, R1–R29 (1985).
14. M. Sheik-Bahae, D. C. Hutchings, D. J. Hagan, and E. W. Van Stryland, "Dispersion of bound electron nonlinear refraction in solids," IEEE J. Quantum Electron. **27**, 1296–1309 (1991).
15. M. Dinu, "Dispersion of phonon-assisted nonresonant third-order nonlinearities," IEEE J. Quantum Electron. **39**, 1298–1503 (2003).
16. G. P. Agrawal, *Nonlinear Fiber Optics*, 2nd ed. (Academic, 1995).
17. D. Modotto, J. P. Mondia, S. Linden, H. W. Tan, R. Morandotti, T. C. Kleckner, A. Locatelli, C. D. Angelis, H. M. v. Driel, C. R. Stanley, and J. S. Aitchison, "Asymmetric spectrum evolution of high power short pulses in AlGaAs," Opt. Commun. **249**, 201–208 (2005).
18. D. C. Hutchings, J. S. Aitchison, B. S. Wherrett, G. T. Kennedy, and W. Sibbett, "Polarization dependence of ultrafast nonlinear refraction in an AlGaAs waveguide at the half-band gap," Opt. Lett. **20**, 991–993 (1995).
19. A. Villeneuve, J. U. Kang, J. S. Aitchison, and G. I. Stegeman, "Unity ratio of cross- to self-phase modulation in bulk AlGaAs and AlGaAs/GaAs multiple quantum well waveguides at half the band gap," Appl. Phys. Lett. **67**, 760–762 (1995).
20. G. I. Stegeman, "Material figures of merit and implications to all-optical waveguide switching," Proc. SPIE **1852**, 75–89 (1993).
21. M. Dinu, F. Quochi, and H. Garcia, "Third-order nonlinearities in silicon at telecom wavelengths," Appl. Phys. Lett. **82**, 2954–2956 (2003).
22. K. Tajima, S. Nakamura, and Y. Sugimoto, "Ultrafast polarization-discriminating Mach–Zehnder all-optical switch," Appl. Phys. Lett. **67**, 3709–3711 (1995).